THE RAIL'S RESPONSE TO THE ACTION OF VERTICAL SLIDING FORCE

Tr. MAZILU*

Este prezentat răspunsul unei şine pe traverse sub acţiunea unei forţe verticale alunecătoare constante sau armonice. Şina este o grindă infinită de tip Timoshenko rezemată pe semitraverse rigide cu trei grade de libertate. Pentru mişcările longitudinale şina este tratată ca o bară simplă. Soluţia ecuaţiilor de mişcare se obţine prin aplicarea metodei funcţiilor Green temporale. Influenţa vitezei asupra rigidităţii dinamice a şinei este prezentată. Se demonstrează că mişcările verticale ale roţilor unui boghiu pot fi cuplate prin undele de încovoiere care se transmit prin şină. Practic, acest cuplaj nu apare la frecvenţe joase, ci la frecvenţe mai mari decât frecvenţa de rezonanţă vârf la vârf.

This article presents the response of a rail track to the action of a vertical sliding force. The dynamic model of railway track is presented, incorporating the rail as an infinite Timoshenko beam, discreetly supported by semi-sleepers with three d. o. f. s. For longitudinal dynamics, the rail is treated as a simple bar. The solution of the motion equations may be obtained by using Green's functions. The influence of velocity on the dynamic stiffness of the rail is presented as well. It is also demonstrated that the vertical movements of the wheels in a bogie may be related through the bend waves that are transmitted through the rail. Practically, this relation does not appear at low frequencies but at frequencies that are superior to the so called 'pinned-pinned resonance frequency'.

Keywords: Rail, bending wave, vertical sliding force

Introduction

The vertical wheel-rail vibrations may be caused by various factors, such as: irregularities of the wheel/rail rolling surfaces, wheel/rail discontinuities (rail joints, crossings, wheel flats, etc.), the variation of dynamic stiffness caused by the sleeper passing, etc. The vertical vibrations may damage the rolling quality and noise emission. They may also lead to rail corrugation.

Basically, the level of wheel-rail vibrations is related to the mechanical characteristics of both, wheel and rail track. As far as it concerns the rail, the main factors are the rail, sleeper and rail-pad characteristics. In order to study the dynamics of the wheel-rail system, the characteristics above could be reflected by the rail's response to a unitary vertical force. The force may be considered as

* Lecturer, Dept. of Railway Vehicles, University "Politehnica"of Bucharest, Romania

constant or harmonic. Two behaviours captured our attention: the force having a fixed support and, the second – a constant speed sliding force.

Practically, the first behaviour is justified because the propagation speed of the free bend waves through the rail is significantly higher than the train velocity. This particular behaviour is used when the vibration frequency is higher than the sleeper-passing frequency and it suites best to the model with a moving irregularity between a stationary wheel and rail. Remington [1] and Thompson [2] used this kind of model in frequency domain for noise prediction.

The second behaviour is specifically adapted to the 'wheel rolling on rail' model. The response of a rail track to sleeper-passing may be studied using this model. Hempelmann [3] has calculated the wheel-rail interaction force in the time domain, at different wheel velocities. After a modal decomposition of the rail and the wheel set he has integrated the differential equations using a modal time-step procedure.

The rail may be described through the finite element method or through analytic models. For example, Nielsen uses finite elements of Rayleigh-Timoshenko beam type. He studies the influence of the irregularities of the wheel/rail rolling surfaces on the vertical loads at different running velocities [4] or calculates the rail corrugation [5].

The rail analytic modeling is based on the Euler-Bernoulli beam or on the Timoshenko beam as well. The Euler-Bernoulli beam has a simpler equation, which can be used successfully only in the low frequencies range. In works [6, 7, 8], the Euler-Bernoulli beam model is used for studying the ground vibrations generated by the vertical interaction wheel/rail forces.

The Timoshenko beam considers the influence of the rotary inertia and shear. The rail could be considered as a Timoshenko beam [3, 9, and 10] or even two Timoshenko beams [11, 12] at medium and high frequencies.

Most of the related works were adopting the hypothesis that the motions of the two rails are uncoupled. Consequently, the rail track is reduced to a rail supported by semi-sleepers that are considered to be inertial elements in vertical translation. The rail pad and the ballast bed are represented each other as elastic and damping paralleled elements of linear characteristics.

The vertical response of the rail supported by concrete sleepers is characterized by two resonance frequencies caused by the rail/sleeper inertial effect. The rail and the sleepers form a two layer elastic oscillating system. Between the two resonance frequencies, the rail's vertical vibration has its own anti-resonance frequency. That is because the sleepers are becoming a vibration absorber. At frequencies in the range of 700 – 1000 Hz (depending on the rail type and the distance between two sleepers - span), the rail's vibration behaviour is characterized by the 'pinned-pinned' resonance frequency, if the harmonic excitation force is applied between two sleepers. The wavelength of the rail's

bend wave equals to twice the span. If the excitation force is applied on the sleeper, the rail's response will be characterized by an anti-resonance which is slightly higher than the 'pinned-pinned' frequency. The resonance/anti-resonance effect described above is the main cause of the short wavelength rail corrugation. The whole mechanism is described in [5].

Mazilu [10] shows that the rail's bend motions are in fact coupled to the longitudinal motions through the rail-pad. Beyond that, in a harmonic fixed support force behaviour, the resonant pinned-pinned effect could be minimized if the rail-pad would be stiffer along the rail.

This work adopts the rail model presented in [10] and studies the rail's response to a sliding (constant and harmonic) force. In order to calculate the response in the time domain, an original variant of Green functions method is applied.

1. The rail's mathematical model

A linear analytic model of the railway track where the rail is an infinite Timoshenko beam and considers the discrete location of sleeper supports has been developed (fig. 1).

The vertical beam bend-motion - $v(x, t)$ is the vertical displacement, $\theta(x, t)$ is the rotation of the cross-section – is coupled to the longitudinal motion - $u(x, t)$ is the longitudinal displacement – due to the rail-pad; the rail is modeled as an infinite bar. The rail's main characteristics are: the mass per unit length m, the density ρ, the flexural rigidity EI, the shear modulus G, the shear constant κ, the area of the cross-section S.

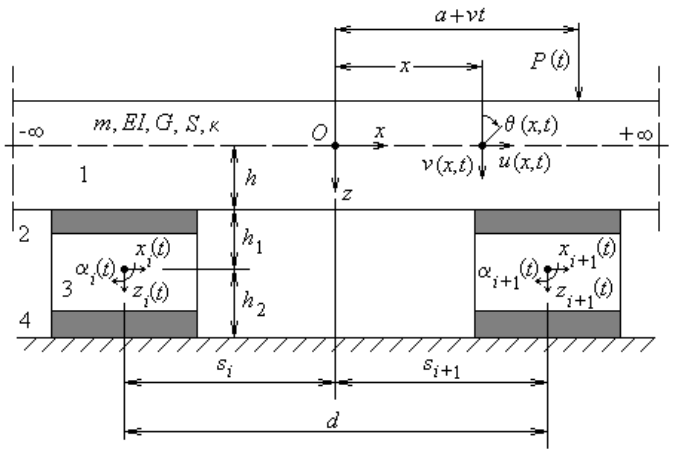

Fig. 1. Mechanical model of track.

1. rail; 2. rail-pad; 3. semi-sleeper; 4. ballast.

The infinite beam has the advantage of eliminating the end-effect that appears in case of using finite beams. Although the numeric simulation will consider a finite number of sleepers, the receptance of rail is periodic along the track and widespread around the considered calculation sector. This aspect is crucial for time-domain integration of the equations of motion, when dealing with a non stationary force.

The semi-sleeper is considered a rigid body with three d. o. f. s.: the vertical translation z_i, the lateral translation x_i (along rail) and the rotation α_i (across rail). A semi-sleeper has the mass M_t and mass-moment of inertia I_t. The place of the sleeper i is s_i.

The rail-pad and the ballast bed are assimilated to elastic and damping elements with linear characteristics. The elastic constants k_{rx}, k_{rz} and $k_{r\alpha}$ and the damping constants c_{rx}, c_{rz} and $c_{r\alpha}$ are related to rail-pad. The stiffness k_{bx}, k_{bz} and the viscous damping constants c_{bx}, c_{bz} refer to the ballast.

A vertical sliding force $P(t)$ that moves with the v velocity in time t is considered to act on the rail. The force is situated at a a distance from the Oxz referential in the initial moment.

The equations of motion may be written in matrix form:

$$\mathbf{L}_{x,t}\{\mathbf{q}\}+\sum_{i\in Z}\left(\mathbf{A}_t\{\mathbf{q}_i\}+\mathbf{B}_t\{\mathbf{q}_i^s\}\right)\delta(x-s_i)=\{\mathbf{p}\} \qquad (1)$$

$$\mathbf{C}_t\{\mathbf{q}_i^s\}=\mathbf{D}_t\{\mathbf{q}_i\} \qquad (2)$$

where $\mathbf{L}_{x,t}$, $\mathbf{A}_t$, $\mathbf{B}_t$, $\mathbf{C}_t$ şi $\mathbf{D}_t$ are standing for matrix differentials (see appendix). The rail's displacements in any x section and in $x = s_i$ sections (to 'i' sleeper) are

$$\{\mathbf{q}\}=\{\mathbf{q}(x,t)\}=\left[u(x,t)\quad v(x,t)\quad \theta(x,t)\right]^t,\ \{\mathbf{q}_i\}=\{\mathbf{q}_i(t)\}=\{\mathbf{q}(s_i,t)\}. \qquad (3)$$

The 'i 'semi-sleeper, situated in the $x = s_i$ section has the following displacements:

$$\{\mathbf{q}_i^s\}=\{\mathbf{q}_i^s(t)\}=\left[x_i(t)\quad z_i(t)\quad \alpha_i(t)\right]^t. \qquad (4)$$

The column vector of the external forces is:

$$\{\mathbf{p}\}=P(t)\delta(x-a-vt)\left[0\quad -1\quad 0\right]^t. \qquad (5)$$

The problem could be solved if we assume the hypothesis that at the initial moment, the displacements are considered to be null. The boundary conditions are null at any particular moment, i.e. the rail's displacements are null if $x \to \pm\infty$.

For this particular form of the equations of motion - vertical force only – the solution may be written as follows:

$$\{\mathbf{q}(x,t)\} = -\int_0^t \int_{-\infty}^{\infty} \{\mathbf{g}(x,\xi,t-\tau)\} P(\tau)\delta(\xi - a - v\tau)\mathrm{d}\xi\mathrm{d}\tau = -\int_0^t \{\mathbf{g}(x,a+v\tau,t-\tau)\} P(\tau)\mathrm{d}\tau \quad (6)$$

$$\{\mathbf{q}_i^s(t)\} = -\int_0^t \int_{-\infty}^{\infty} \{\mathbf{g}_i(\xi,t-\tau)\} P(\tau)\delta(\xi - a - v\tau)\mathrm{d}\xi\mathrm{d}\tau = -\int_0^t \{\mathbf{g}_i(a+v\tau,t-\tau)\} P(\tau)\mathrm{d}\tau \quad (7)$$

in which $\{\mathbf{g}(x, \xi, t - \tau)\} = [g^u(x, \xi, t - \tau), g^v(x, \xi, t - \tau), g^\theta(x, \xi, t - \tau)]^t$ stands for the Green functions' column vector for rail displacements and $\{\mathbf{g}^s_i(\xi, t - \tau)\} = [g^x_i(\xi, t - \tau), g^z_i(\xi, t - \tau), g^\alpha_i(\xi, t - \tau)]^t$ stands for the Green functions' column vector for '*i*' sleeper displacements. The Green functions' vector $\{\mathbf{g}(x, \xi, t - \tau)\}$ contains the rail displacements in section '*x*' at the moment $t - \tau > 0$, if at the τ moment in section ξ an impulse force occurred. The Green functions' vector $\{\mathbf{g}^s_i(\xi, t - \tau)\}$ contains the '*i*' sleeper displacement at $t - \tau$ moment, if at the τ moment in section ξ an impulse force occurred.

The Green's functions are the solutions for equations (1-2) if the right term of the first equation is

$$\{\mathbf{p}\} = \delta(x-\xi)\delta(t-\tau)\begin{bmatrix}0 & 1 & 0\end{bmatrix}^t. \quad (8)$$

The Green's functions may be calculated using the Fourier transform

$$\{\mathbf{g}(x,\xi,t-\tau)\} = \frac{1}{2\pi}\int_{-\infty}^{\infty} \{\mathbf{G}(x,\xi,\tau,\omega)\}\exp(\mathrm{j}\omega t)\mathrm{d}\omega = \frac{2}{\pi}\int_0^{\infty} \{\mathrm{Re}\,\mathbf{G}(x,\xi,\tau,\omega)\}\cos\omega t\mathrm{d}\omega \quad (9)$$

$$\{\mathbf{g}_i^s(\xi,t-\tau)\} = \frac{1}{2\pi}\int_{-\infty}^{\infty} \{\mathbf{G}_i^s(\xi,\tau,\omega)\}\exp(\mathrm{j}\omega t)\mathrm{d}\omega = \frac{2}{\pi}\int_0^{\infty} \{\mathrm{Re}\,\mathbf{G}_i^s(\xi,\tau,\omega)\}\cos\omega t\mathrm{d}\omega \quad (10)$$

in which $\mathrm{j}^2 = -1$ and

$$\{\mathbf{G}\} = \{\mathbf{G}(x,\xi,\tau,\omega)\} = \begin{bmatrix}\boldsymbol{G}^u(x,\xi,\tau,\omega) & \boldsymbol{G}^v(x,\xi,\tau,\omega) & \boldsymbol{G}^\theta(x,\xi,\tau,\omega)\end{bmatrix}^t = F[\{\mathbf{g}(x,\xi,t-\tau\}] \quad (11)$$

$$\{\mathbf{G}_i^s\} = \{\mathbf{G}_i^s(\xi,\tau,\omega)\} = \begin{bmatrix}\boldsymbol{G}_i^x(\xi,\tau,\omega) & \boldsymbol{G}_i^z(\xi,\tau,\omega) & \boldsymbol{G}_i^\alpha(\xi,\tau,\omega)\end{bmatrix}^t = F\left[\{\boldsymbol{g}_i^s(\xi,t-\tau\}\right], \quad (12)$$

F [.] is the Fourier transform.

It's easy to observe that the Fourier transform of the Green's functions are:

$$\{\mathbf{G}\} = \exp(-\mathrm{j}\omega\tau)\{\mathbf{Q}\} = \exp(-\mathrm{j}\omega\tau)\begin{bmatrix}\boldsymbol{U}(x,\xi,\omega) & \boldsymbol{V}(x,\xi,\omega) & \boldsymbol{\Theta}(x,\xi,\omega)\end{bmatrix}^t \quad (13)$$

$$\{\mathbf{G}_i^s\} = \exp(-\mathrm{j}\omega\tau)\{\mathbf{Q}_i^s\} = \exp(-\mathrm{j}\omega\tau)\begin{bmatrix}\boldsymbol{X}_i(\xi,\omega) & \boldsymbol{Z}_i(\xi,\omega) & \boldsymbol{A}_i(\xi,\omega)\end{bmatrix}^t, \quad (14)$$

in which the column vectors $\{\mathbf{Q}\}$ and $\{\mathbf{Q}^s_i\}$ are the solutions for the following equations:

$$\mathbf{L}_{x,\omega}\{\mathbf{Q}\}+\sum_{i\in Z}\left(\mathbf{A}_\omega\{\mathbf{Q}_i\}+\mathbf{B}_\omega\{\mathbf{Q}^s_i\}\right)\delta(x-s_i)=\delta(x-\xi)[0\quad 1\quad 0]^t \tag{15}$$

$$\mathbf{C}_\omega\{\mathbf{Q}^s_i\}=\mathbf{D}_\omega\{\mathbf{Q}_i\} \tag{16}$$

where $\{\mathbf{Q}_i\}=[\boldsymbol{U}(s_i,\,\xi,\,\omega)\;\boldsymbol{V}(s_i,\,\xi,\,\omega)\;\boldsymbol{\Theta}(s_i,\,\xi,\,\omega)]^t$ and $\mathbf{L}_{x,\omega}=F[\mathbf{L}_{x,t}]$, $\mathbf{A}_\omega=F[\mathbf{A}_t]$ etc. In the equations above $\boldsymbol{U}$, $\boldsymbol{V}$, $\boldsymbol{\Theta}$, $\boldsymbol{X}_i$, $\boldsymbol{Y}_i$, and $\boldsymbol{A}_i$ are standing for complex value functions.

Depending on $\{\mathbf{Q}_i\}$, the vector $\{\mathbf{Q}^s_i\}$ may be extracted from the last equation. Then, from the first equation the following results:

$$\mathbf{L}_{x,\omega}\{\mathbf{Q}\}=\delta(x-\xi)[0\quad 1\quad 0]^t-\sum_{i\in Z}\mathbf{K}_\omega\{\mathbf{Q}_i\}\delta(x-s_i) \tag{17}$$

with $\mathbf{K}_\omega=\mathbf{A}_\omega+\mathbf{B}_\omega\mathbf{C}^{-1}{}_\omega\mathbf{D}_\omega$.

The $\mathbf{L}_{x,\omega}$ operator may be diagonal led if the equation above is multiplied by the matrix operator

$$\mathbf{J}_x=\begin{bmatrix}1 & 0 & 0\\ 0 & \dfrac{EI}{GS\kappa}\dfrac{\mathrm{d}^2}{\mathrm{d}x^2}+\dfrac{\rho I\omega^2}{GS\kappa}-1 & \dfrac{\mathrm{d}}{\mathrm{d}x}\\ 0 & -\dfrac{\mathrm{d}}{\mathrm{d}x} & \dfrac{\mathrm{d}^2}{\mathrm{d}x^2}+\dfrac{\omega^2 m}{GS\kappa}\end{bmatrix}. \tag{18}$$

The solutions may be written as follows

$$\{\mathbf{Q}\}=\int_{-\infty}^{\infty}\boldsymbol{\Gamma}\left[\mathbf{J}_{x'}\delta(x'-\xi)[0\quad 1\quad 0]^t-\sum_{i\in z}\mathbf{J}_{x'}\delta(x'-s_i)\mathbf{K}_\omega\{\mathbf{Q}_i\}\right]\mathrm{d}x' \tag{19}$$

where $\boldsymbol{\Gamma}$ stands for the diagonal operator's Green's functions matrix

$$\mathbf{L}^*_{x,\omega}=\mathbf{J}_x\mathbf{L}_{x,\omega}=\begin{bmatrix}ES\dfrac{\mathrm{d}^2}{\mathrm{d}x^2}+m\omega^2 & 0 & 0\\ 0 & H_x & 0\\ 0 & 0 & H_x\end{bmatrix} \tag{20}$$

with

$$H_x = EI\frac{\mathrm{d}^4}{\mathrm{d}x^4} + \omega^2\left(m\frac{EI}{\kappa SG} + \rho I\right)\frac{\mathrm{d}^2}{\mathrm{d}x^2} + m\omega^2\left(\frac{\rho\omega^2 I}{\kappa SG} - 1\right).$$

The $\mathbf{\Gamma}$ matrix of Green's functions is the solution of the following equation:

$$\mathbf{L}^*_{x,\omega}\mathbf{\Gamma} = \delta(x - x')\mathbf{E}, \tag{21}$$

where $\mathbf{E}$ stands for the 3 x 3 unity matrix.

The $\mathbf{\Gamma}$ matrix has the following shape:

$$\mathbf{\Gamma} = \begin{bmatrix} \Gamma^u(x,x',\omega) & 0 & 0 \\ 0 & \Gamma^v(x,x',\omega) & 0 \\ 0 & 0 & \Gamma^\theta(x,x',\omega) \end{bmatrix} \tag{22}$$

in which the Green's functions are [10]

$$\Gamma^u(x,x',\omega) = \mathrm{j}\frac{\exp\left(-\mathrm{j}\beta|x - x'|\right)}{2\beta SE}$$

$$\Gamma^v(x,x',\omega) = \Gamma^\theta(x,x',\omega) = -\frac{\beta_2\exp\left(-\beta_1|x - x'|\right) + \mathrm{j}\beta_1\exp\left(-\beta_2|x - x'|\right)}{2\beta_1\beta_2(\beta_1^2 + \beta_2^2)EI}$$

where

$$\beta = \sqrt{\frac{m\omega^2}{SE}} \text{ and } \beta_{1,2} = \sqrt{\sqrt{\frac{\rho^2\omega^4}{4E^2}\left(\frac{E}{G\kappa} - 1\right)^2 + \frac{m\omega^2}{EI}} \mp \frac{\rho\omega^2}{2E}\left(\frac{E}{G\kappa} + 1\right)}.$$

The calculation for rail displacements near the *'k'* sleeper is going to be done by the use of (19) in which $\{\mathbf{Q}\}$ will be replaced by $\{\mathbf{Q}_k\}$. Thus, the following will result:

$$\{\mathbf{Q}(s_k,\xi,\omega)\} = \{\mathbf{P}_k\} - \sum_{i\in Z}\mathbf{\Gamma}^*(s_k,s_i,\omega)\mathbf{K}_\omega\{\mathbf{Q}(s_i,\xi,\omega)\}, \tag{23}$$

where

$$\{\mathbf{P}_k\} = \mathbf{\Gamma}^*(s_k,\xi,\omega)\begin{bmatrix}0 & 1 & 0\end{bmatrix}^t; \mathbf{\Gamma}^*(s_k,\xi,\omega) = \int_{-\infty}^{\infty}\mathbf{\Gamma}(s_k,x',\omega)\mathbf{J}_{x'}\delta(x'-\xi)\mathrm{d}x'.$$

Finally, by considering a number of n sleepers (with n sufficiently as large), the following matrix equation results:

$$\begin{bmatrix} \mathbf{E}-\mathbf{\Gamma}^*_{1,1}\mathbf{K}_\omega & \mathbf{\Gamma}^*_{1,2}\mathbf{K}_\omega & \dots & \mathbf{\Gamma}^*_{1,n}\mathbf{K}_\omega \\ \mathbf{\Gamma}^*_{2,1}\mathbf{K}_\omega & \mathbf{E}-\mathbf{\Gamma}^*_{2,2}\mathbf{K}_\omega & \dots & \mathbf{\Gamma}^*_{2,n}\mathbf{K}_\omega \\ \dots & \dots & \dots & \dots \\ \mathbf{\Gamma}^*_{n,1}\mathbf{K}_\omega & \mathbf{\Gamma}^*_{n,2}\mathbf{K}_\omega & \dots & \mathbf{E}-\mathbf{\Gamma}^*_{n,n}\mathbf{K}_\omega \end{bmatrix} \begin{bmatrix} \{\mathbf{Q}_1\} \\ \{\mathbf{Q}_2\} \\ \dots \\ \{\mathbf{Q}_n\} \end{bmatrix} = \begin{bmatrix} \{\mathbf{P}_1\} \\ \{\mathbf{P}_2\} \\ \dots \\ \{\mathbf{P}_n\} \end{bmatrix} \tag{24}$$

with $\mathbf{\Gamma}^*_{i,k} = \mathbf{\Gamma}^*(s_i, s_k, \omega)$.

2. Numerical application

Further on, the particular case of a rail track consisting in a rail having the linear mass m = 56 kg/m on concrete sleepers, is studied. The values for the involved parameters are: $I = 23.14 \cdot 10^{-6}$ m^4, $S = 7.134 \cdot 10^{-3}$ m^2, E = 210 GPa, G = 85 GPa, $\kappa = 0.34$, M_s = 129 kg, $I_s = 0.82$ kgm^2, $d = 0.698$, $h = 0.08$ m , $h_1 = 0.085$ m, $h_2 = 0.089$ m, $k_{rx} = 34$ MN/m, $k_{rz} = 280$ MN/m, $k_{r\alpha} = 114.3$ kNm, $c_{rx} = 24$ kNs/m, c_{rz} = 63 kNs/m, $c_{r\alpha} = 25.7$ Nms, $k_{bx} = 35$ MN/m, $k_{bz} = 180$ MN/m, $c_{bx} = 52$ kNs/m, and c_{bz} = 82 kNs/m. The magnitude of vertical force is P = 1N.

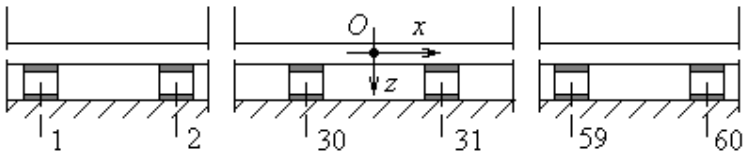

Fig. 2. The schema for numeric simulation.

This original numerical application considers a track sector of n = 60 sleepers with the referential originating in its middle (see Fig. 2). The vertical force displaces itself between the initial abscissa point a and the final abscissa point, b. The calculation covered the rail displacement at the half of the distance between two sleepers (point 'O') and right above a sleeper (sleeper #31).

The integration time step was chosen as Δt = 1/40000 s, no matter how high the vertical force displacement speed was. According to that, the ξ coordinate along the rail was discreet with the step of $\Delta\xi = v\Delta t$. The (9) integration was numerically calculated using the 3rd degree spleen functions in a frequency range of 0 to 2200 Hz.

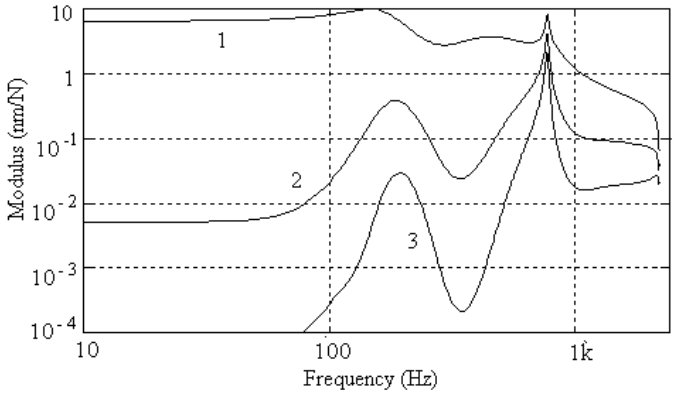

Fig.3. The receptance of rail between two sleepers.

Fig. 3 displays the frequency response of the rail's vertical displacement in the origin point in the range of 10 – 2200 Hz. Three particular cases were considered: the harmonic excitation force applied in the origin point (curve 1), five sleepers away (curve 2) and ten sleepers away (curve 3). In the first case, the response was dominated by the rail's resonance frequency and the two elastic layers (the rail-pad and the ballast). This was calculated for f = 148 Hz. The response was additionally dominated by the pinned – pinned resonance frequency caused by the sleeper-passing effect (f = 772 Hz). In the last other cases, the receptance of rail reached its maximum at the pinned – pinned resonance frequency.

The damping of the rail vibrations increases along with the distance between the point of force application and the receptance calculation point. This damping is high in the range of low and medium frequencies and significantly low at high frequencies.

Fig. 4 displays the receptance of rail just above one sleeper. Curve 1 is corresponding to excitation above the sleeper, curve 2 – the harmonic force at a distance of 10 sleepers away from the calculation point and curve 3 – excitation at 9 ½ sleepers, between the sleepers. It is to notice that the anti-resonance effect occurred near the sleeper considered for calculation and that the anti-resonance frequency is slightly higher than the pinned-pinned frequency. If the harmonic force is applied at a certain distance from the considered calculation point, the frequency response is dominated by the pinned-pinned resonance frequency. This indicates that the rail has a certain tendency to transmit the bend waves corresponding to this frequency.

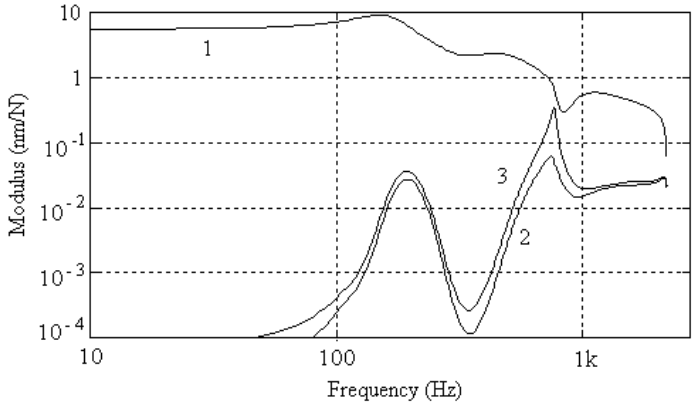

Fig.4. The receptance of rail over a sleeper.

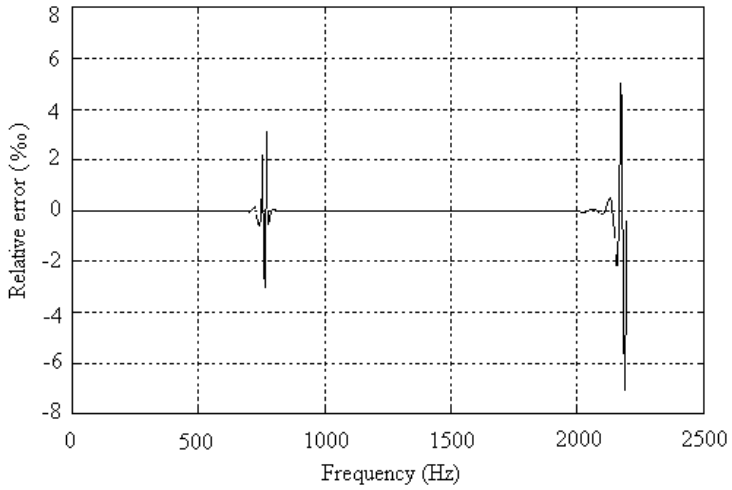

Fig.5. The relative error between the receptance of rail calculated between 10 sleepers from the origin and the one calculated in the origin

Fig. 5 displays the relative error between the receptance of rail calculated between the sleepers #39 and #40 and the one calculated in the origin; the excitation force was applied near the calculation receptance point. Minor differences appeared at the resonance frequency only and that is due to the sleeper-passing effect (under 0.3 %) and at the maximum calculus frequency (under 0.7 %). As a result, the proposed rail model will keep the periodic character for the rail's frequency response along the considered calculation sector.

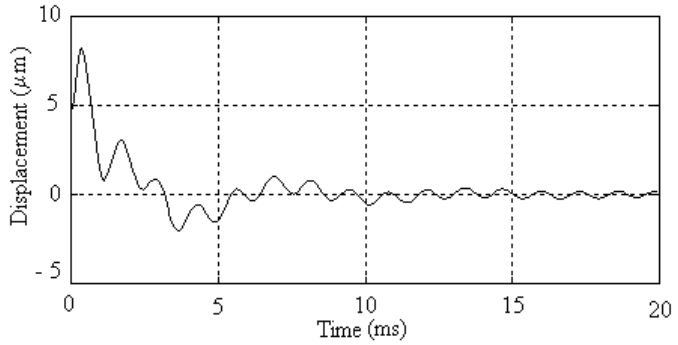

Fig. 6. The Green's function $g^v(0, 0, t)$.

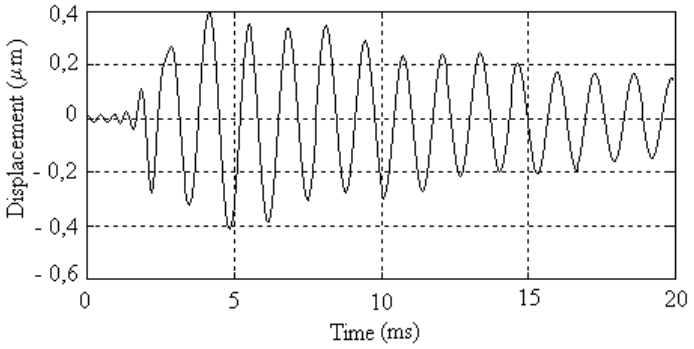

Fig.7. The Green's function $g^v(0, - 4{,}2, t)$.

Figs. 6 and 7 are displaying the Green's temporal function for the rail's vertical displacement. The vertical rail displacement in the origin point 'O', was calculated at the moment $\tau = 0$, when the impulse force occurs (see Fig. 6) and at a distance of 6 sleepers away (see Fig. 7). The maximum vertical rail displacement decreases along with the increase of the distance where the initial impulse is applied, from 8.2 μm to 0.42 μm respectively. By observing Fig. 6, it is to notice that two oscillations corresponding to the respective resonance frequencies are coexisting. The damping of the vibration occurs pretty fast. If the impulse is applied at a greater distance (Fig. 7), the rail's vibration begins practically with a delay caused by the propagation of the impulse along the rail from the application point to the calculation point. The rail vibration is dominated by the pinned – pinned resonance frequency's component. The damping is much slower this time.

The Green's function calculated near the 31st sleeper when the impulse is applied there and, respectively, at a distance of 6 sleepers away is presented in Figs. 8 and 9. The values are smaller then the ones calculated at half distance between two sleepers. In both simulated situations, the rail vibration is quickly damped.

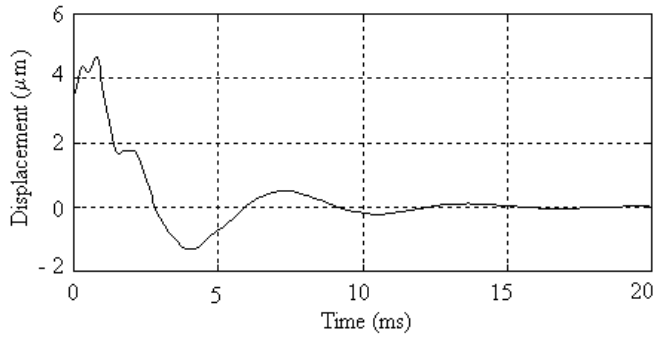

Fig. 8. The Green's function $g^v(0{,}35,\ 0{,}35,\ t)$.

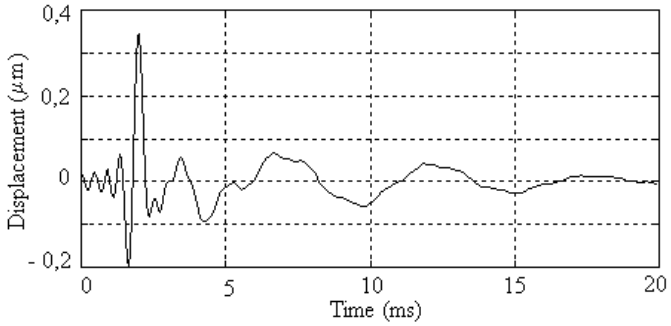

Fig. 9. The Green's function $g^v(0{,}35,\ -3{,}85,\ t)$.

Fig. 10 displays the rail's vertical displacement calculated in the origin point while a constant sliding force (with its magnitude of 1 N) passes with a velocity of 40 m/s. The movement begins at a distance of 6 sleepers away from the calculation point (a = - 4,2 m and b = 4,2 m). At the beginning of the force displacement, the rail will enter a transitory behaviour. After 50 – 60 ms, the transitory behaviour is damped and the rail's deformation resembles with the one corresponding to the static load behaviour. The displacement variation is practically symmetric, using a correct approximation. The maximal value for the displacement is 6.57 nm.

A similar evolution may be observed in Fig. 11, which shows the rail's displacement calculated near sleeper #31. The force is also constant and passes at a velocity of 40 m/s. Though, the rail's maximum displacement is smaller due to the sleeper's vertical withstanding. Its value is 5.63 nm.

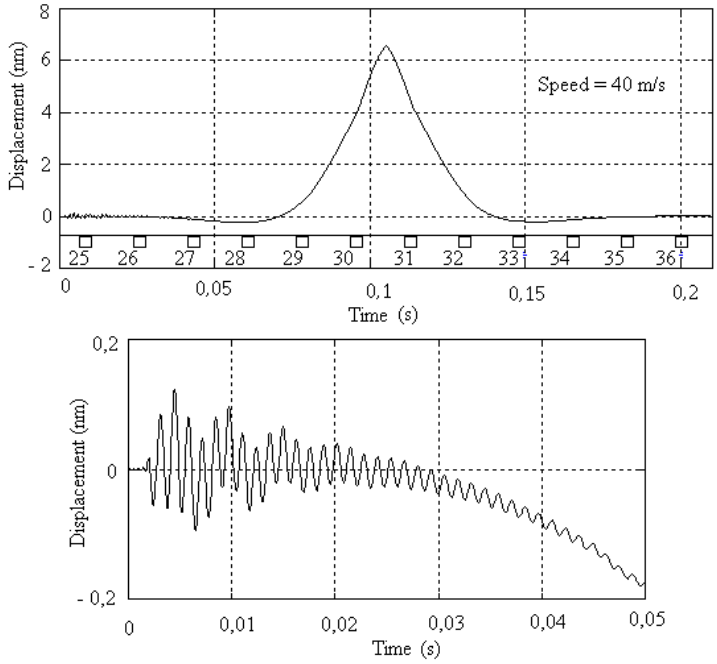

Fig. 10. The rail displacement at half the distance between two sleepers under a constant sliding force (with its magnitude of 1 N).

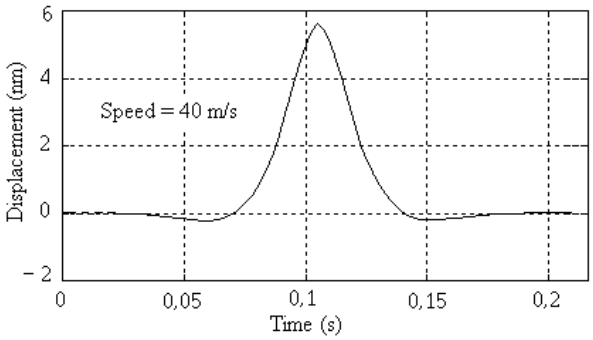

Fig. 11. The rail displacement over a sleeper under a constant sliding force (with its magnitude of 1 N).

The calculation is showing that together with the increase of the velocity, the rail's maximum displacement at half the distance between two sleepers is also increasing. The static deformation at half the distance between two sleepers is 6.44 nm and for a constant sliding force (with its magnitude of 1 N) which passes with a velocity of 80 m/s, the displacement is 6.62 nm. Thus, the dynamic stiffness decreases because the sliding force's velocity is close to the bend wave

propagation speed according to the first resonance. This particular aspect explains partially that the track is overloaded along with the increase of the running speeds.

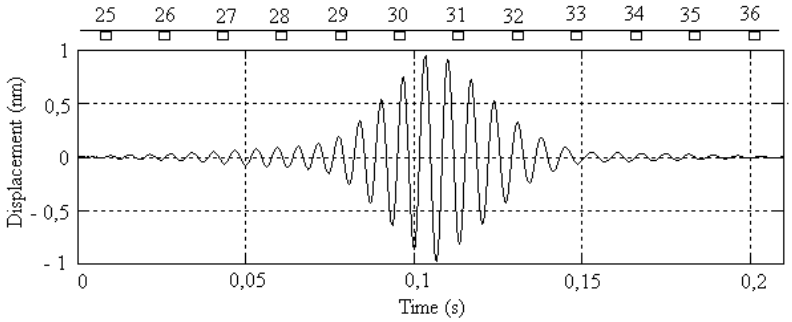

Fig. 12. The rail displacement at half the distance between two sleepers under a harmonic sliding force (speed 40 m/s, frecquency 148 Hz).

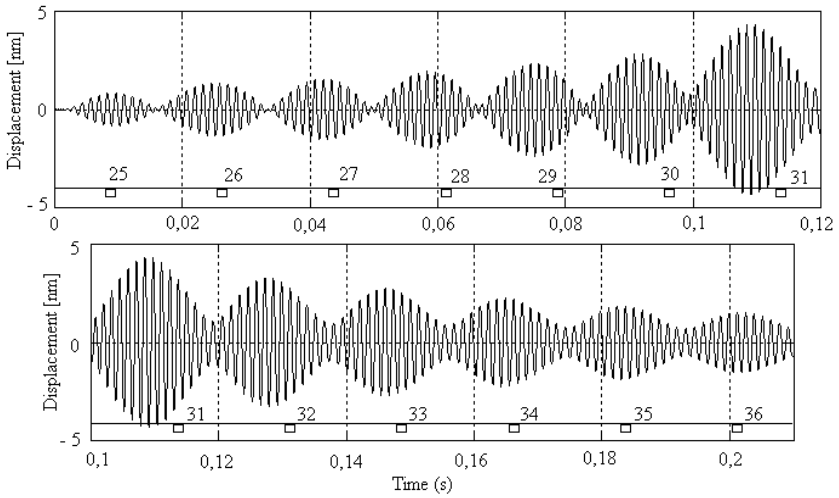

Fig. 13. The rail displacement at half the distance between two sleepers under a harmonic sliding force (speed 40 m/s, frecquency 772 Hz).

Figs. 12 and 13 are displaying the rail's response at half the distance between two sleepers when a harmonic sliding force (with its amplitude of 1 N) passes. Two frequencies were considered – one equal to 148 Hz (fig. 12) and the other one equal to 772 Hz (fig. 13). If the excitation force has a frequency of 148 Hz, the rail's amplitude increases as the force approaches the calculation point. The sleepers do not influence the rail vibration in a significant matter. The time history is symmetric. The maximum amplitude is practically equal to the one calculated for the fixed support harmonic force. The rail's vibration increases and decreases its intensity when the force is situated at a distance equal to twice the span from the calculation point.

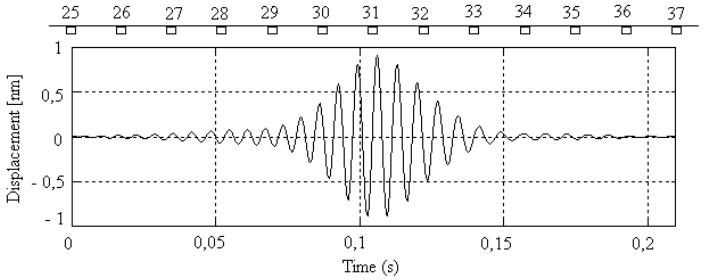

Fig. 14. The rail displacement over a sleeper under a harmonic sliding force (speed 40 m/s, frecquency 148 Hz).

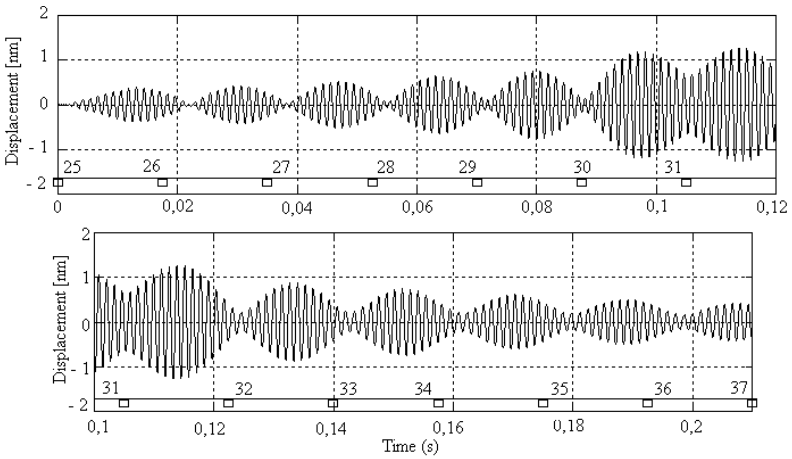

Fig. 15. The rail displacement over a sleeper under a harmonic sliding force (speed 40 m/s, frecquency 772 Hz).

If the excitation force has a frequency of 772 Hz – the pinned – pinned resonance – then the rail's maximum displacement is smaller than the one calculated for the fixed support harmonic force (fig. 3). As a result, the maximum amplitude was 4.3 nm, compared to 8.5 nm for the one calculated for the fixed support harmonic force.

The rail's vibration begins intensively way earlier than the harmonic force has reached the calculation point, between sleepers #30 and #31, respectively. The rail vibration is highly modulated due to the sleepers. At this frequency, the wavelength is equal to twice the span. It is also important to notice a specific delay which decreases as the force approaches from the calculation point. At the beginning of the force movement, the vibration peak is reached when passing over a sleeper. The rail displacement's history is no longer symmetrical, but clearly asymmetrical. The rail vibration lasts longer after the force has passed.

Similar evolutions were noticed when passing over a sleeper with a harmonic force (with its amplitude of 1 N) at a speed of 40 m/s and frequencies of 148 Hz and 772 Hz respectively (see Figs. 14 and 15).

Conclusions

The knowledge of the rail's response to the action of a vertical sliding force (constant or sinusoidal) is useful in solving specific problems such as: rail track dynamics, rolling quality, noise emission and rail corrugation occurrence.

The complex dynamic model of railway track was presented, incorporating the rail as an infinite Timoshenko beam, discreetly supported by semi-sleepers with three d. o. f. s. The coupling of bend motions together to the longitudinal ones was considered. The Green's (temporal) functions method was used for solving the movement equations. These were calculated numerically, starting from the Green's harmonic response functions.

The infinite beam has the advantage of that preserves the periodicity of the receptance of rail on a long distance.

The numeric results showed that under a constant sliding load, the rail's maximum displacement increases along with the force speed, which is in accordance to the experimental observations.

The rail's response to the action of a vertical sinusoidal sliding force is selective depending on the frequency. At low frequencies, the response is not influenced by the sleepers. The rail vibration as well, begins and ends practically when the excitation force is close to the calculation point. For the studied rail characteristics, the influence distance is approximately the span. Usually, the bogie wheelbase is 1.8 m for freight cars and 2.5 – 2.6 m for passenger cars. Thus, the bend waves could not reach from a wheel to another. The wheels may be considered as uncoupled.

At the pinned – pinned resonance frequency and at high frequencies, the rail's response is influenced by the sleeper positions. The rail vibration begins way earlier than the harmonic force has reached the calculation point. The rail continues to vibrate long after the force has passed. In this particular situation, a bogie's wheels are coupled through the bend waves propagating through the rail.

The results are quite similar to the ones corresponding to the fixed support force. These aspects influence the rail's acoustic radiation. Thus, some discrepancies from the above mentioned situation occur. As a conclusion, is the fact that the rail's dynamic response may be calculated more accurately.

R E F E R E N C E S

1. *Remington, J. P.* Wheel/rail rolling noise – part I: theoretical analysis. In: Journal of the Acoustical Society of America 81 1805-1823, 1987.
2. *Thompson, D. J.* Wheel – rail noise generation, Part I: introduction and interaction model. In: Journal of Sound and Vibration, 161(3), 387-400, 1993.
3. *Hempelmann, K., Ripke, B., Dietz, S.* Modelling the dynamic interaction of wheel set and track. In: Railway Gazette International, 591 – 595, Sept. 1992.

4. *Nielsen, J.C.O., Igeland, A.* Vertical dynamic interaction between train and track-influence of wheel and track imperfections. In: Journal of Sound and Vibration 187 (1995) 825-739.
5. *Nielsen, J.C.O.* Numerical prediction of rail roughness growth on tangent railway tracks. In: Journal of Sound and Vibration 267 (2003) 537-548.
6. *Sheng, X., Jones, C.J.C., Petyt, M.* Ground vibration generated by a load moving along a railway track. In: Journal of Sound and Vibration 228 (1999) 129-156.
7. *Jones, C.J.C., Sheng, X., Petyt, M.* Simulation of ground vibration from a moving harmonic load on a railway track. In: Journal of Sound and Vibration 231 (2000) 739-751.
8. *Sheng, X., Jones, C.J.C., Thompson, D.J.* A theoretical model for ground vibration from trains generated by vertical track irregularities. In: Journal of Sound and Vibration 272 (2004) 937-965.
9. *Grassie, S. L., Gregory, R. W., Harrison, D., Johnson, K. L.* The dynamic response of railway track to high frequency vertical excitation. In: Journal Mechanical Engineering Science, 2, 77 - 90, 1982.
10. *Mazilu, Tr.* Propagation of harmonic vertical waves in a rail. In: Scintific Bulletin Series D : Mechanical Engineering, vol. 67 no. 2 (2005) 99-110.
11. *Wu, T. X., Thompson, D.J.* A double Timoshenko beam model for vertical vibration analysis of railway track at high frequencies. In: Journal of Sound and Vibration 224 (2) (1999) 329-348.
12. *Wu, T. X., Thompson, D.J.* On parametric excitation of the wheel/track system. In: Journal of Sound and Vibration 278 (2004) 725-747.

APPENDIX

The differential matrix operators from the movement equations (1) and (2) are:

$$\mathbf{L}_{x,t}=\begin{bmatrix} ES\dfrac{\partial^2}{\partial x^2}-m\dfrac{\partial^2}{\partial t^2} & 0 & 0 \\ 0 & GS\kappa\dfrac{\partial^2}{\partial x^2}-m\dfrac{\partial^2}{\partial t^2} & -GS\kappa\dfrac{\partial}{\partial x} \\ 0 & GS\kappa\dfrac{\partial}{\partial x} & EI\dfrac{\partial^2}{\partial x^2}-GS\kappa-\rho I\dfrac{\partial^2}{\partial t^2} \end{bmatrix},$$

$$\mathbf{A}_{t}=\begin{bmatrix} -c_{rx}\dfrac{\mathrm{d}}{\mathrm{d}t}-k_{rx} & 0 & h\left(c_{rx}\dfrac{\mathrm{d}}{\mathrm{d}t}+k_{rx}\right) \\ 0 & -c_{rz}\dfrac{\mathrm{d}}{\mathrm{d}t}-k_{rz} & 0 \\ h\left(c_{rx}\dfrac{\mathrm{d}}{\mathrm{d}t}+k_{rx}\right) & 0 & -(c_{r\alpha}+h^2c_{rx})\dfrac{\mathrm{d}}{\mathrm{d}t}-k_{r\alpha}-h^2k_{rx} \end{bmatrix},$$

$$\mathbf{B}_t = \begin{bmatrix} c_{rx}\dfrac{\mathrm{d}}{\mathrm{d}t} + k_{rx} & 0 & h_1\left(c_{rx}\dfrac{\mathrm{d}}{\mathrm{d}t} + k_{rx}\right) \\ 0 & c_{rz}\dfrac{\mathrm{d}}{\mathrm{d}t} + k_{rz} & 0 \\ -h\left(c_{rx}\dfrac{\mathrm{d}}{\mathrm{d}t} + k_{rx}\right) & 0 & (c_{r\alpha} - hh_1c_{rx})\dfrac{\mathrm{d}}{\mathrm{d}t} + k_{r\alpha} - hh_1k_{rx} \end{bmatrix},$$

$$C_t = \begin{bmatrix} M_s\dfrac{\mathrm{d}^2}{\mathrm{d}t^2} + c_{sx}\dfrac{\mathrm{d}}{\mathrm{d}t} + k_{sx} & 0 & \Delta c\dfrac{\mathrm{d}}{\mathrm{d}t} + \Delta k \\ 0 & M_s\dfrac{\mathrm{d}^2}{\mathrm{d}t^2} + c_{sz}\dfrac{\mathrm{d}}{\mathrm{d}t} + k_{sz} & 0 \\ \Delta c\dfrac{\mathrm{d}}{\mathrm{d}t} + \Delta k & 0 & I_s\dfrac{\mathrm{d}^2}{\mathrm{d}t^2} + c_{s\alpha}\dfrac{\mathrm{d}}{\mathrm{d}t} + k_{s\alpha} \end{bmatrix}$$

with

$$c_{sx} = c_{rx} + c_{bx};\ c_{sz} = c_{rz} + c_{bz};\ c_{s\alpha} = c_{r\alpha} + h_1^2c_{rx} + h_2^2c_{bx};$$
$$\Delta c = h_1c_{rx} - h_2c_{bx};$$

$$k_{sx} = k_{rx} + k_{bx};\ k_{sz} = k_{rz} + k_{bz};\ k_{s\alpha} = k_{r\alpha} + h_1^2k_{rx} + h_2^2k_{bx};$$

$$\Delta k = h_1k_{rx} - h_2k_{bx}$$

and

$$\mathbf{D}_t = \begin{bmatrix} c_{rx}\dfrac{\mathrm{d}}{\mathrm{d}t} + k_{rx} & 0 & -h\left(c_{rx}\dfrac{\mathrm{d}}{\mathrm{d}t} + k_{rx}\right) \\ 0 & c_{rz}\dfrac{\mathrm{d}}{\mathrm{d}t} + k_{rz} & 0 \\ h_1\left(c_{rx}\dfrac{\mathrm{d}}{\mathrm{d}t} + k_{rx}\right) & 0 & (c_{r\alpha} - hh_1c_{rx})\dfrac{\mathrm{d}}{\mathrm{d}t} + k_{r\alpha} - hh_1k_{rx} \end{bmatrix}.$$